2012

Computational fluid dynamics investigation of the orientation of a pediatric left ventricle assist device cannula to reduce stroke events

Stephen Guimond
University of Central Florida

COMPUTATIONAL FLUID DYNAMICS INVESTIGATION OF THE ORIENTATION OF A PEDIATRIC LEFT VENTRICLE ASSIST DEVICE CANNULA TO REDUCE STROKE EVENTS

by

STEPHEN A. GUIMOND

A thesis submitted in partial fulfillment of the requirements

for the Honors in the Major Program in Mechanical Engineering

in the College of Engineering and Computer Science

and in The Burnett Honors College

at the University of Central Florida

Orlando, Florida

Fall Term 2012

Thesis Chair: Dr. Alain Kassab

ABSTRACT

Ventricle Assist Devices (VADs), which are typically either axial or centrifugal flow pumps implanted on the aortic arch, have been used to support patients who are awaiting cardiac transplantation. Success of the apparatus in the short term has led to long term use. Despite anticoagulation measures, blood clots (thrombi) have been known to form in the device itself or inside of the heart. The Ventricle Assist Devices supply blood flow via a conduit (cannula) implanted on the ascending aorta. Currently, the implantation angle of the VAD cannula is not taken into consideration. Since the VADs supply a significant amount of blood flow to the aorta, the implantation angle can greatly affect the trajectory of the formed thrombi as well as the cardiac flow field inside of the aortic arch. This study aims to vary the implantation angle of a pediatric Left Ventricle Assist Device (LVAD) through a series of computational fluid dynamics (CFD) software simulations focusing on the aortic arch and its branching arteries of a 20 kg pediatric patient in order to reduce the occurrence of stroke.

ACKNOWLEDGEMENTS

I would like to thank Dr. Alain Kassab for guiding me along the way to Honors Thesis and undergraduate research completion. I would also like to thank ThuyTien Nguyen and Lauren Blanchette for helping with meshing and gathering data. Finally, I would like to thank my parents for giving me opportunity and the tools necessary to succeed.

TABLE OF CONTENTS

LIST OF FIGURES

LIST OF TABLES

CHAPTER 1: INTRODUCTION

Ventricle Assist Devices (VADs), which are typically either axial or centrifugal flow pumps implanted on the aortic arch, have been used to support patients who are awaiting cardiac transplantation. Success of the apparatus in the short term has led to long term use. Despite anticoagulation measures, blood clots (thrombi) have been known to form in the device itself or inside of the heart. Once the clots pass through the VAD, they are free to flow through the aortic arch and have the possibility of entering the carotid and vertebral arteries causing stroke or death.

The Ventricle Assist Devices supply blood flow via a conduit (cannula) implanted on the ascending aorta. Currently, the implantation angle of the VAD cannula is not taken into consideration. Since the VADs supply a significant amount of blood flow to the aorta, the implantation angle can greatly affect the trajectory of the formed thrombi as well as the cardiac flow field inside of the aortic arch. This study aims to vary the implantation angle of a pediatric Left Ventricle Assist Device (LVAD) through a series of computational fluid dynamics (CFD) software simulations focusing on the aortic arch and its branching arteries of a 20 kg pediatric patient in order to reduce the occurrence of stroke. The simulations use a synthetic representation of typical pediatric aortic arch geometry. The CFD simulations are carried out using ANSYS FLUENT 12.1.4 with post-processing done in Paraview 3.14.1.

CHAPTER 2: LITERATURE REVIEW

VADs originally were only used as an intermediate step for patients awaiting cardiac transplant as bridge-to-transplantation therapy but successful transplants led to a more long term use consideration for VAD technology. As a result, VAD design has significantly improved long term survival rates for pediatric patients. Despite the improvements, VAD patients still suffer from thrombi formation that has the potential to cause permanent damage or death.

Typical Pediatric Mechanical Circulatory Assist Devices Available

Over its history, Extracorporeal Membrane Oxygenation (ECMO) has been the most commonly used form of assist device dating back to its first successful use in 1975 (Kormos et al.) and totals more than 3,500 uses in pediatric cases (Duncan). Because of the extracorporeal nature, ECMO has also been one of the few support devices used for infant patients.

In terms of VADs, the Bio-Pump (by the Medtronic Corporation) has been the most frequently used device for pediatric patients in the United States (Duncan). The device is a centrifugal, steady flow system specifically designed to be able to be used in pediatrics and the device offers convenience and pump priming advantages over ECMO. The Bio-Pump is also adaptable in that it can be used on newborn to adult patients (Duncan).

One of the most successful pediatric VADs for use in Europe is the Berlin Heart VAD that has the ability to be used on neonates as well as pediatric patients. This axial flow, pulsatile VAD has only been used on 50 cases in North America due to its limited availability. The Berlin Heart VAD is the most promising VAD for pediatrics and offers a larger survivability rate than the Bio-Pump and ECMO.

The Micromed DeBakey VAD Child is a modified adult DeBakey VAD made suitable for pediatrics. The device is implantable and only recommended for children in the age range of 5 to 16 years. Due to the intracorporeal functionality of the device, the body surface areas of patients are restricted to the range of 0.7 and 1.5 m^2 (Duncan) as neonatal patients don't offer enough room to house the mechanism.

Device Success Rates

Despite being the most commonly used mechanical support method ECMO is only suitable for short term use because of the high 60% mortality rates (Duncan). Reports in the 1970s show that significant instances of bleeding and thrombosis occurred in the pediatric patients studied (Kormos et al.). The Bio-Pump suffers from the same mortality rates as ECMO. A study carried out between 2001 and 2008 involving a total of 42 pediatric patients (21 received ECMO, 21 received Berlin Heart VAD) of similar weight and age states that ECMO patients had an average survival rate of 57% with 15 ± 12 days of support while Berlin Heart VAD patients had an average survival rate of 86% with 42 ± 43 days of support (Imamura et al.).

A report in 2006 by Fraser et al. details the only 6 uses of the DeBakey Pediatric VAD at that time. The patients had an average age of 11.3 years and average duration of support of 39 days. Two of the noted patients had significant coagulation complications denoted by increased pump requirement and one of the two complications ended in death. Of the 6 total cases, 3 were successfully transplanted while the remaining three died during support resulting in a 50% survival rate.

A Previous CFD Study in VAD Orientation (Osorio et al.)

The implication that the orientation of a VAD cannula can be optimized to reduce stroke occurrence is a relatively new idea. Recently, a study by Osorio et al. focused on the cannula implantation angle of an LVAD using representative adult aortic arch geometry. The thrombi were modeled as spheres with diameters of 2, 3 and 5 mm. The study used three different cannula orientations of 0^o, 30^o, and 60^o (measured off of the normal to the cannula implantation site) as well as two different bypass scenarios per cannula orientation. The bypass conduits are installed below the cannula implantation site and proceed to either the innominate artery (IA, called AO-IA bypass) or the left carotid artery (LCA, called AO-LCA bypass). The bypasses are intended to eliminate stroke events originating from the IA and LCA by delivering thrombus-free blood from below the cannula implantation site to the respective arteries.

The resulting simulations show that changing the orientation of the LVAD cannula can have a large impact on the flow field developed within the aortic arch. Orientation angles of 0^o and 30^o showed a noticeable flow recirculation zone due to cannula outflow jet impingement on the opposing wall of the ascending aorta while the 60^o orientation caused the cannula outflow to be delivered to the base of LCA with very little flow recirculation. In all cases there was a region of flow separation and recirculation at the entrance to the descending aorta which has the potential for clot formation. The study shows that it is possible to reduce the overall occurrence of stroke by 50% when a no bypass, 60^o LVAD cannula orientation is used. Unfortunately, the aortic bypass scenarios only showed minimal reduction in stroke occurrence. It is worth noting that an orientation that resulted in stroke reduction for 5 mm particles did not necessarily result in a stroke reduction for 2 mm particles. This is due to the tendency of smaller particles to

follow flow streamlines while larger particles are less inclined to change their trajectory when encountering flow redirections.

CHAPTER 2: METHODS

Computational Fluid Dynamics

Computational fluid dynamics software is a great tool for engineering design and analysis. Proposed designs for fluid systems such as turbine blades, airfoils and HVAC systems can be easily and affordably analyzed without the need to build a physical scale test model. By solving conservation of mass, conservation of energy and the Navier-Stokes momentum equations in a discrete manner, CFD can predict the velocity, pressure and temperature fields for a given flow geometry and can be used for incompressible, compressible and reacting or non-reacting flow regimes. CFD makes use of a computational grid (called a mesh) and transforms a real, continuous fluid region into discrete fluid elements called control volumes. The governing equations are transformed into algebraic equations and are solved at the specific control volume locations created by the mesh.

There are many CFD codes available but this study specifically makes use of the finite-volume commercial code ANSYS FLUENT 12.1.4. Flow through the aortic arch is assumed incompressible and any heat transfer is neglected. This study focuses on the steady state behavior of the flow field and neglects the pulsatile nature of the cardiac output. VAD manufacturers state that VADs are operated with a 30% pulsatility variance (maximum flow rate minus minimum over the baseline value) which is small enough so that a steady simulation will yield appropriate results (Osorio et al.). A sick heart only outputs a fraction of its healthy flow rate and so the pulsatility originating from the heart will be greatly reduced. As a result of these

simplifications, only the conservation of mass (Eq. 1) and momentum equations (Eq. 2) must be solved.

$$\nabla \cdot \vec{v} = 0 \qquad \text{(Eq. 1)}$$

$$\rho(\vec{v} \cdot \nabla \vec{v}) = -\nabla p + \mu \nabla^2 \vec{v} + \rho \vec{g} \qquad \text{(Eq. 2)}$$

Note that (Eqs. 1-2) are formulated in a rectangular coordinate system and v is the velocity vector, ρ is the fluid density, p is the pressure, μ is the fluid dynamic viscosity and g is the gravitational acceleration vector.

Flow leaving both the heart and VAD are considered turbulent so the CFD simulations must incorporate a turbulence model. The two main turbulence models used in computational fluid simulations are the k-ε and k-ω models which both calculate time-averaged values of truly transient flow properties. The k-ε model considers the factors that affect the turbulent kinetic energy (k) and turbulent dissipation rate (ε). If the k-ε model is to be used, the improved Realizable k-ε is chosen because of its better prediction of boundary layers under adverse pressure gradients or strong separation, rotation, recirculation and strong streamline curvature (Bakker). The k-ε model is good for core turbulent flow but it relies on empirical wall functions based on flat plate behavior to approximate what occurs to the fluid at walls. Wall functions result in a lower mesh size and smaller computation time but the model may not be appropriate for all flows. The k-ω model is similar to the k-ε model but it uses a modified form of the equation for k and does not use wall functions. An improved version, the k-ω Shear Stress Transport (SST) model is a hybrid: the fluid behavior is modeled near the wall with the k-ω equations and the fluid far away from the wall is modeled with the k-ε equations and a blending

function is used to connect the two models. As such, it requires higher mesh resolution near the walls and thus larger computational time however the payoff is better prediction of fluid behavior near walls. In order to accurately resolve cardiac flow fields, the k-ω SST turbulence model was used.

Pediatric LVAD Cardiac Geometry

The pediatric aortic arch follows the same general shape as an adult aortic arch except the dimensions are scaled down. Following blood flow from the left ventricle as shown in Figure 1, the ascending aorta (AO) first encounters the innominate artery (IA) which branches into the right subclavian artery (RSA), right vertebral artery (RVA) and right carotid artery (RCA). The flow next encounters the left carotid artery (LCA) and the left subclavian artery (LSA) which branches into the left vertebral artery (LVA). The aortic arch ends with the descending aorta (DA) which supplies blood to the lower extremities.

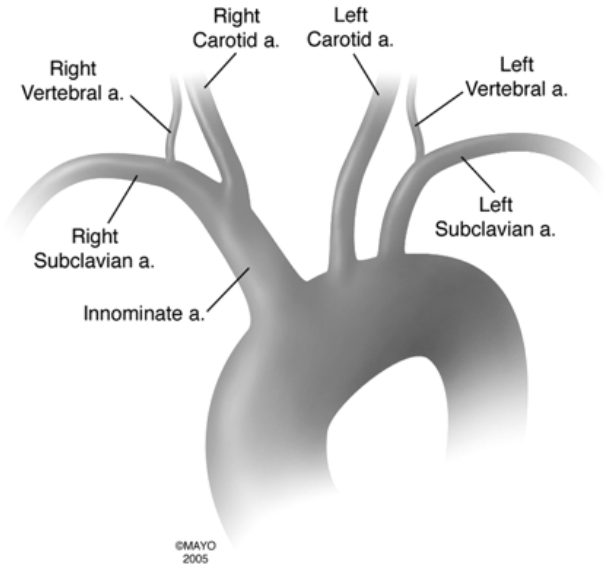

Figure 1: Most common aortic arch in humans (Layton)

Representative vessel dimensions were chosen to create the three dimensional pediatric model (Solidworks 2010) for use in the CFD simulations.

Three different LVAD ascending aorta implantation angles were studied: the standard LVAD perpendicular ($\beta = 90^{o}$) orientation along with an intermediate ($\beta = 60^{o}$) and shallow ($\beta = 30^{o}$) orientation. The standard perpendicular orientation with model dimensions is shown in Figure 2 and the three orientations are shown in Figure 3.

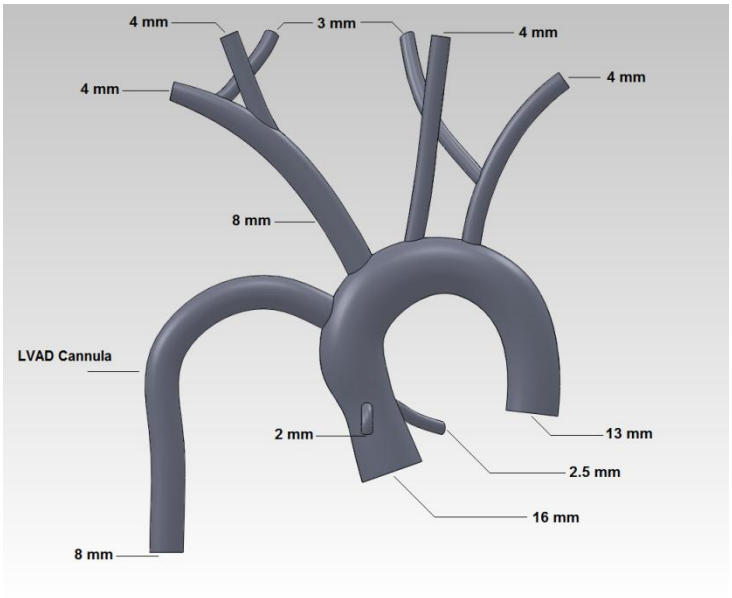

Figure 2: 3D model and dimensions

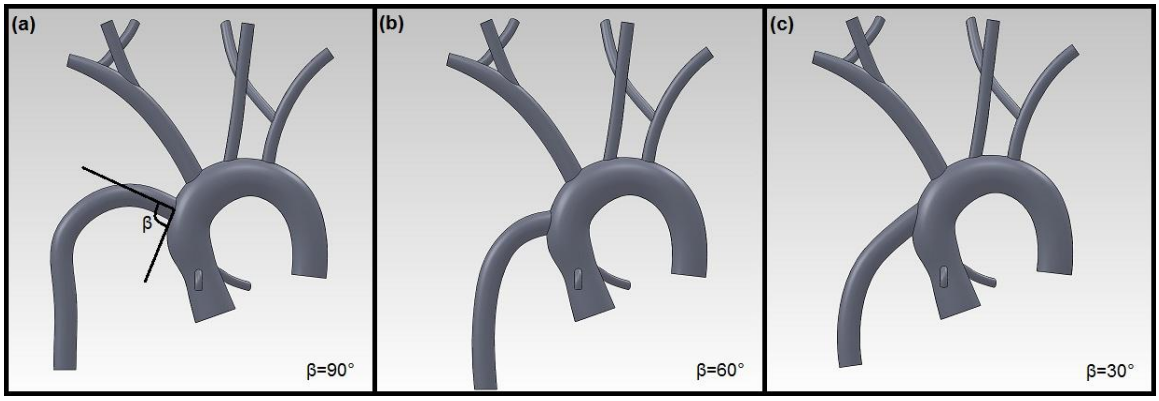

Figure 3: 3D models for the three β orientations used

In addition, two bypass scenarios (IA and LCA bypass) for each LVAD orientation were considered. The bypasses are intended to eliminate the presence of thrombi in either the IA or the LCA by rerouting thrombus free ascending aorta flow. The 3D models for the bypasses are shown on a perpendicular LVAD configuration in Figure 4. These configurations result in a total of 9 cases: 3 different implantation angles with three different bypass scenarios (no bypass, AO-IA bypass, AO-LCA bypass) per implantation angle.

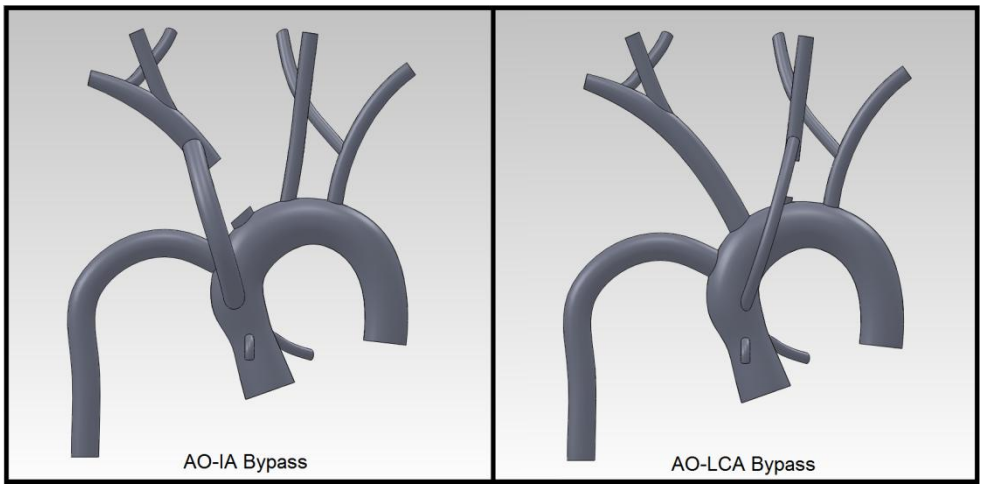

Figure 4: 3D model for both IA and LCA bypass scenarios

Meshing

The philosophy used to mesh the cardiac geometry was twofold:

1. Include enough grid points to capture boundary layer behavior
2. Grow cells gradually into the core of the flow

Pointwise (Gridgen) was used for mesh generation and tetrahedral element geometry was chosen due to its flexibility in capturing geometry. In order to judge the quality of the meshes, cell equivolume skewness, equiangle skewness and aspect ratio were monitored. If too many elements have values that fall too close to 1 (equivolume, equiangle skewness) or are too large (aspect ratio) inaccuracies will be present in the CFD simulation. In order to properly capture boundary layer behavior, near wall element sizes were kept small as to resolve the large velocity gradients. Smaller velocity gradients in the core flow allowed for much larger element sizes than the near wall region. Figure 5 shows the tetrahedral surface mesh and Figure 6 shows the tetrahedral volume mesh for the $\beta = 90^{o}$ no bypass case. All of the cases follow the same mesh generation procedure.

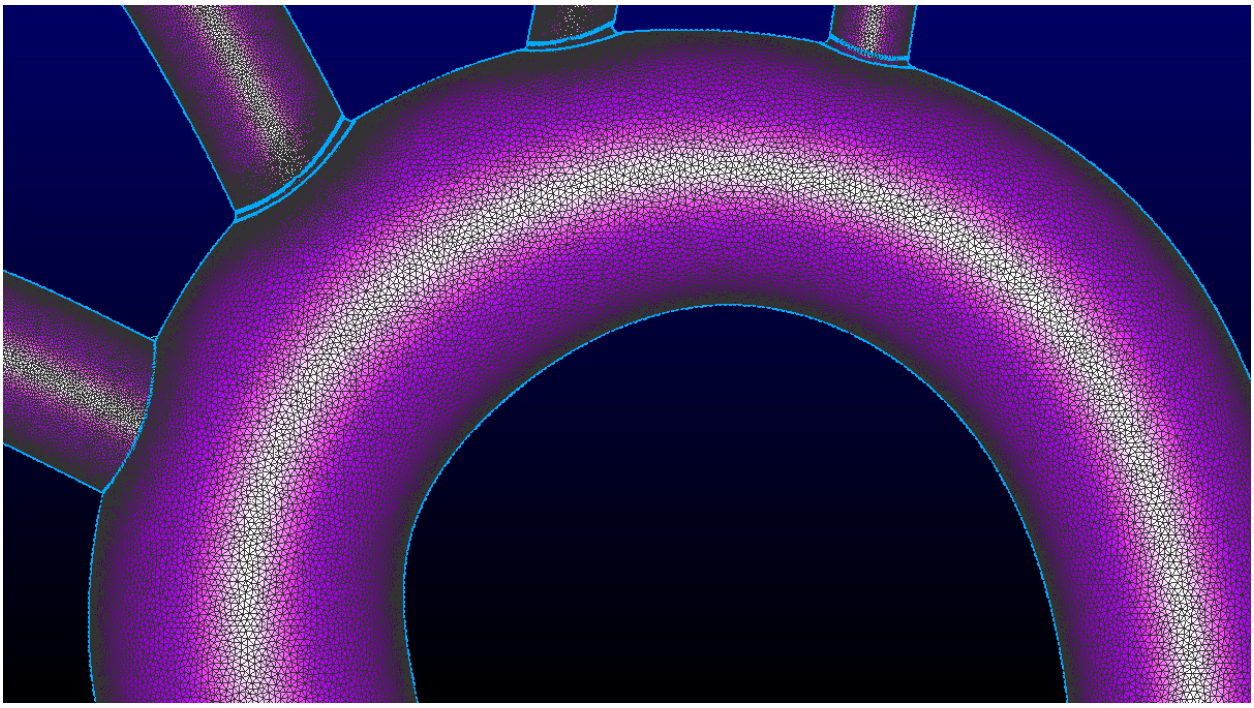

Figure 5: Tetrahedral surface mesh for β = 90° no bypass

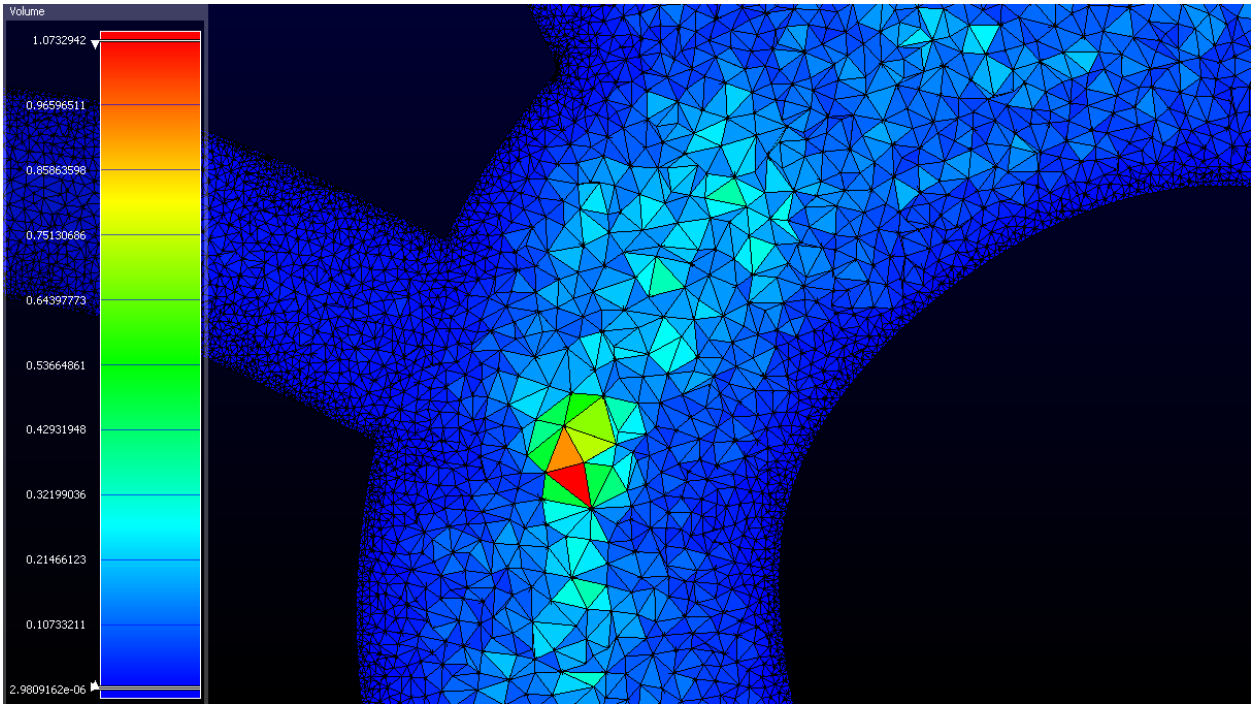

Figure 6: Tetrahedral volume mesh for β = 90° no bypass

In order to judge how well the mesh characterizes the turbulent boundary layer behavior, the y+ value during the CFD simulation was monitored. The y+ value is defined as

$$y^+ = \frac{u^* y}{\nu}$$

where u* is the friction velocity, y is the normal distance from the wall, and ν is the kinematic viscosity of the fluid. The friction velocity is defined as

$$u^* = \sqrt{\frac{\tau_w}{\rho}}$$

where τ_w is the wall shear stress and ρ is the fluid density. The y+ value is a normalized value and is usually plotted against the fluid velocity normalized by the friction velocity; this quantity is referred to as u+. When plotted, the relation looks like Figure 7 (Bakker).

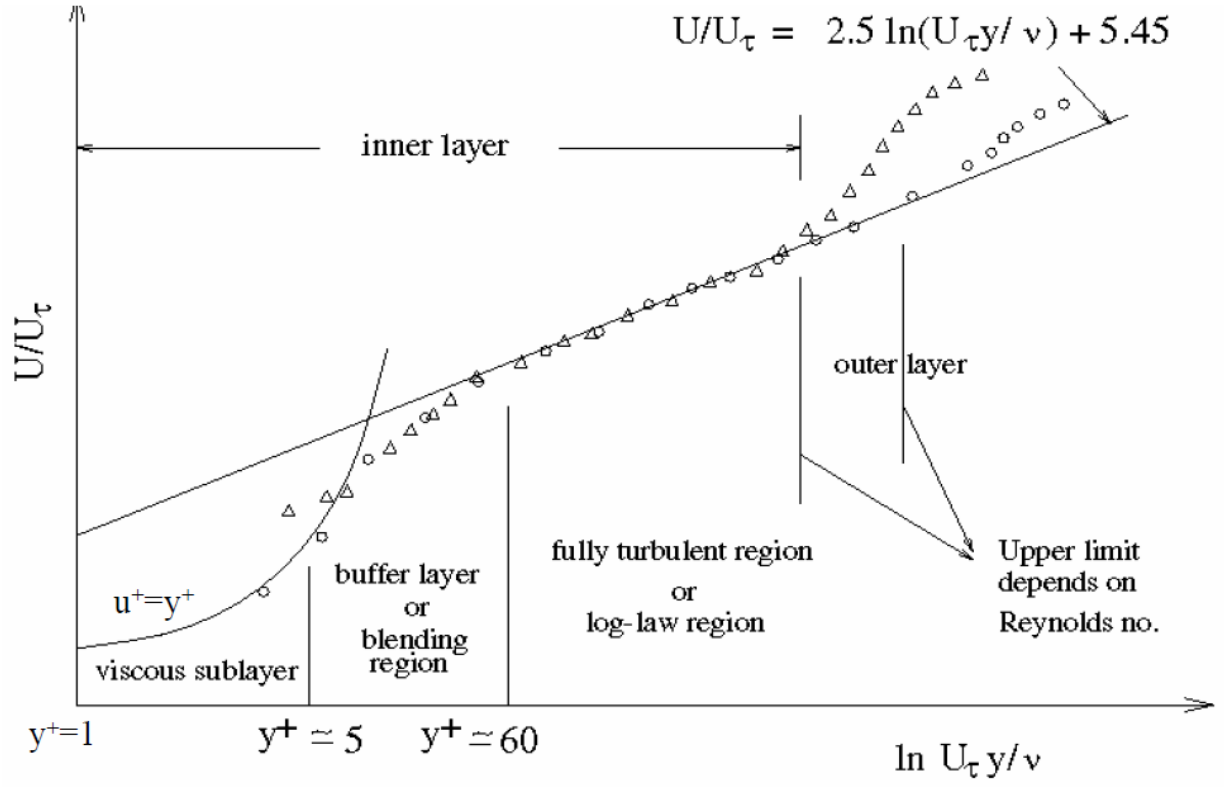

Figure 7: Boundary layer structure (Bakker)

It can be seen that the boundary layer can be separated into four regions: the viscous sub layer, the buffer layer, the fully turbulent region and the outer layer. In order to accurately capture the boundary layer using the k-ω SST turbulence model, the first grid point from the wall must be placed in the viscous sub layer (y+ < 5) and the grid should ideally have a y+ value of about 1. Figure 8 shows contours of the wall y+ for the perpendicular case and it can be seen that the values are well within the appropriate limits. It should be noted that you cannot calculate a y+ value without a fluid velocity so in this aspect the mesh generation is iterative. Once appropriate element sizes were chosen for one case, the same sizes could be comfortably used on the remaining LVAD configuration meshes.

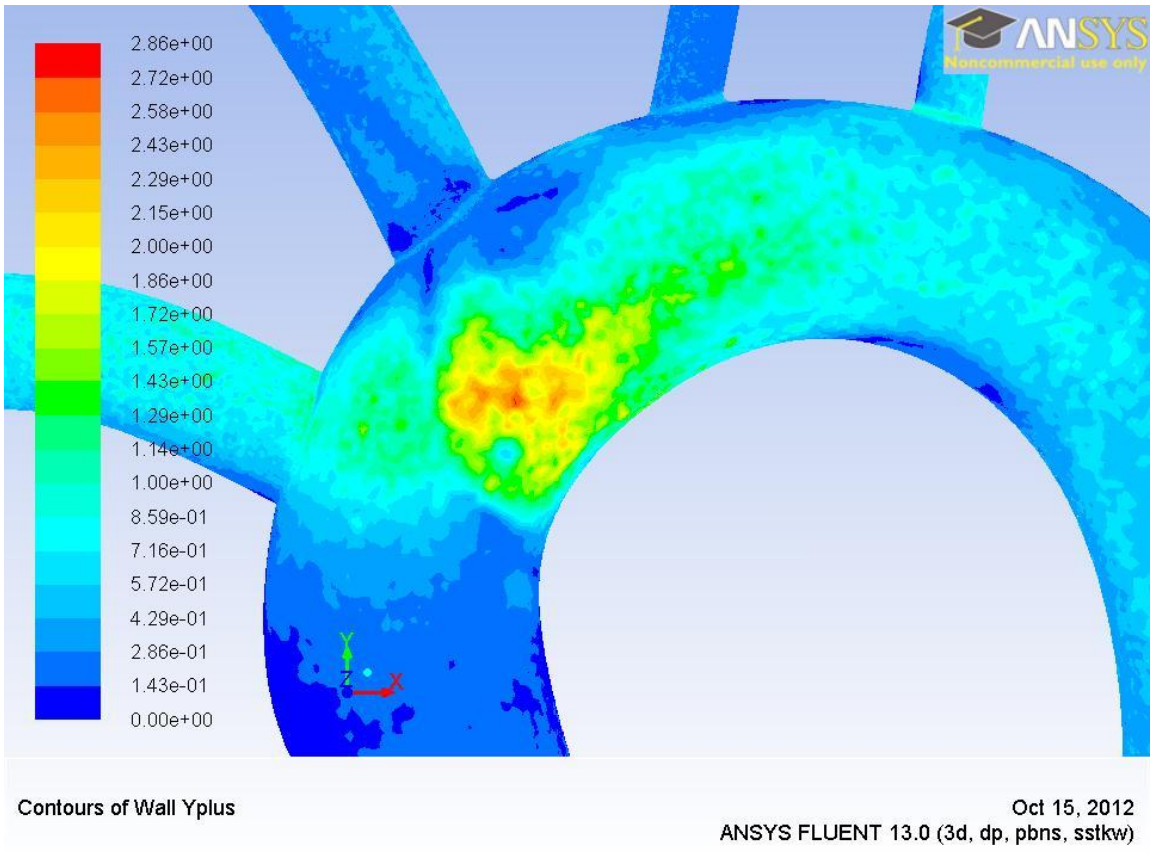

Figure 8: Contours of wall y+ for β = 90° no bypass

The average value of all the final meshes was calculated to be about 5.3 million tetrahedral elements. A grid convergence study was conducted using the β = 90° no bypass case by increasing and decreasing the total number of mesh elements by 15% and running the two simulations. Fluid pressure and velocity values were taken at the vessel exits as well as overall maximum pressure and velocity values and compared to the base mesh. It was found that the maximum percent change between the coarser and finer mesh variants (over all pressure and velocity values) was 2.69%. Therefore confidence can be taken in the grid independence of the calculated velocity field and thrombi destinations.

CHAPTER 3: RESULTS

Once the cardiac flow field is calculated, thrombi are randomly released from the inlet plane of the LVAD cannula. The thrombi are modeled as non-interacting spheres of 1, 2, 3 and 4 mm diameter. Thrombus destinations were then statistically analyzed over five separate release trials per diameter using a 95% confidence level. The trajectories of the thrombi are calculated using a Lagrangian formation momentum balance that includes particle inertia and fluid drag force (ANSYS FLUENT). The buoyancy force seen by the thrombi in blood is assumed minimal due to similar density values ($\rho = 1116.73$ kg/m^3 for thrombus and $\rho = 1060$ kg/m^3 for blood) so it was neglected. The thrombi destination results signifying stroke (embolization of the LCA, RCA or Vertebrals) are summarized in Table 1 and the flow fields for the three no bypass cases are shown in Figure 9.

Table 1: Percentage of Thrombi Embolizing to Carotid and Vertebral Arteries (mean±SD)

	Thrombi Size						
					Overall*		
Configuration	1 mm	2 mm	3 mm	4 mm	Carotids	Vertebrals	Total
β=90°: No Bypass	19.67±0.48	18.39±0.92	10.78±0.56	9.27±0.89	10.77±0.33	3.75±0.79	14.53±0.74
+ AO-IA Bypass	24.45±0.73	18.94±1.36	11.79±0.53	12.11±1.26	12.74±0.45	4.08±0.92	16.82±1.03
+ AO-LCA Bypass	14.54±0.81	13.83±0.41	9.8±0.54	10.28±0.54	8.3±0.53	3.82±0.45	12.12±0.59
β=60°: No Bypass	20.75±0.4	18.19±0.63	11.42±0.65	9.28±0.44	10.47±0.32	4.44±0.31	14.91±0.54
+ AO-IA Bypass	21.16±0.51	18.36±1.01	12.55±0.37	11.9±0.62	13.18±0.42	2.81±0.58	15.99±0.67
+ AO-LCA Bypass	19.98±1.39	16.75±0.43	11.55±0.7	10.97±0.18	9.64±0.3	5.18±0.78	14.82±0.81
β=30°: No Bypass	16.1±0.22	11.24±0.43	2.57±0.15	4.91±0.29	6.65±0.22	2.05±0.23	8.7±0.29
+ AO-IA Bypass	14.29±0.45	11.92±0.99	4.25±0.38	6.33±0.22	6.26±0.39	2.94±0.32	9.2±0.59
+ AO-LCA Bypass	10.9±0.36	8.21±0.58	5.05±0.33	11.31±1.04	5.47±0.42	3.39±0.53	8.87±0.64

AO=aorta, IA=innominate artery, LCA=left carotid artery, SD=standard deviation. *set of all 20 particle release simulations for each configuration. Configurations have statistically significantly different overall percentages (χ^2=3925, df=11, p<0.0001).

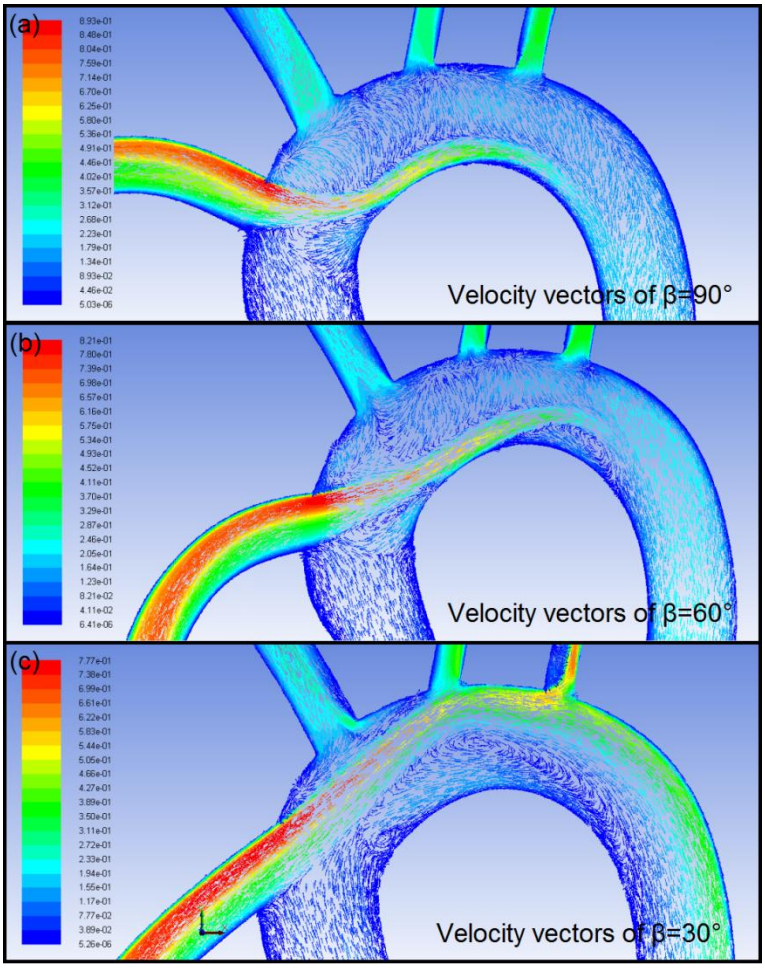

Figure 9: Velocity vectors for the β = 90°, 60° and 30° no bypass cases

It can be seen from Table 1 that all of the β = 90° and β = 60° cannula orientation cases resulted in significantly worse stroke probabilities when compared to the β = 30° orientation. In both of those cases, the cannula is directed such that significant recirculation is generated when the cannula outflow impinges on the inner aortic wall (see Figure 9a and 9b). The particles become entrained in this recirculation zone and have the ability to end up in the IA as well as the LCA. Interestingly, the β = 90° (standard) and β = 60° orientation average very similar total

embolization probabilities at 14.49% and 15.24%, respectively. This is likely due to the "re-randomization" that occurs when the particles enter the recirculation zones.

It's obvious that an LVAD orientation of $\beta = 30^o$ offers the greatest reduction in stroke occurrence. At this orientation, Figure 9c shows that cannula outlet flow avoids the inner aortic wall completely and impinges on the outer aortic wall between the takeoff for the LCA and LSA. While it appears from the flow field that a large portion of thrombi would enter the LCA, the 30^o orientation results in a noticeable carotid embolization reduction.

The intent of both the AO-IA and AO-LCA bypasses is to eliminate thrombi from entering the respective vessels by feeding thrombus-free blood straight from the ascending aorta. The results for $\beta = 90^o$ and $\beta = 60^o$ cases show that the bypass cases offered minimal improvement, if any, when compared to the standard $\beta = 90^o$ LVAD orientation. The cannula flow recirculation zones created in these cases are responsible for that outcome. Comparing Figure 4 with Figure 9a it can be seen that the bypass implantation locations on the aortic wall sit directly over the recirculation zone created in the $\beta = 90^o$ orientation and the entrained particles are transported to either the IA or the LCA directly.

The bypass cases for the $\beta = 30^o$ orientation offer no advantage or disadvantage over the no bypass case due to the fact that a cannula flow recirculation zone is not created. However, the 30^o orientation does cause a significant flow reversal throughout the apex of the aortic arch. Once caught in this zone, particles completely reverse their trajectory and are reintroduced into the cannula flow further upstream. A smaller region of flow is stagnant inside of this larger recirculation could cause additional thrombi formation.

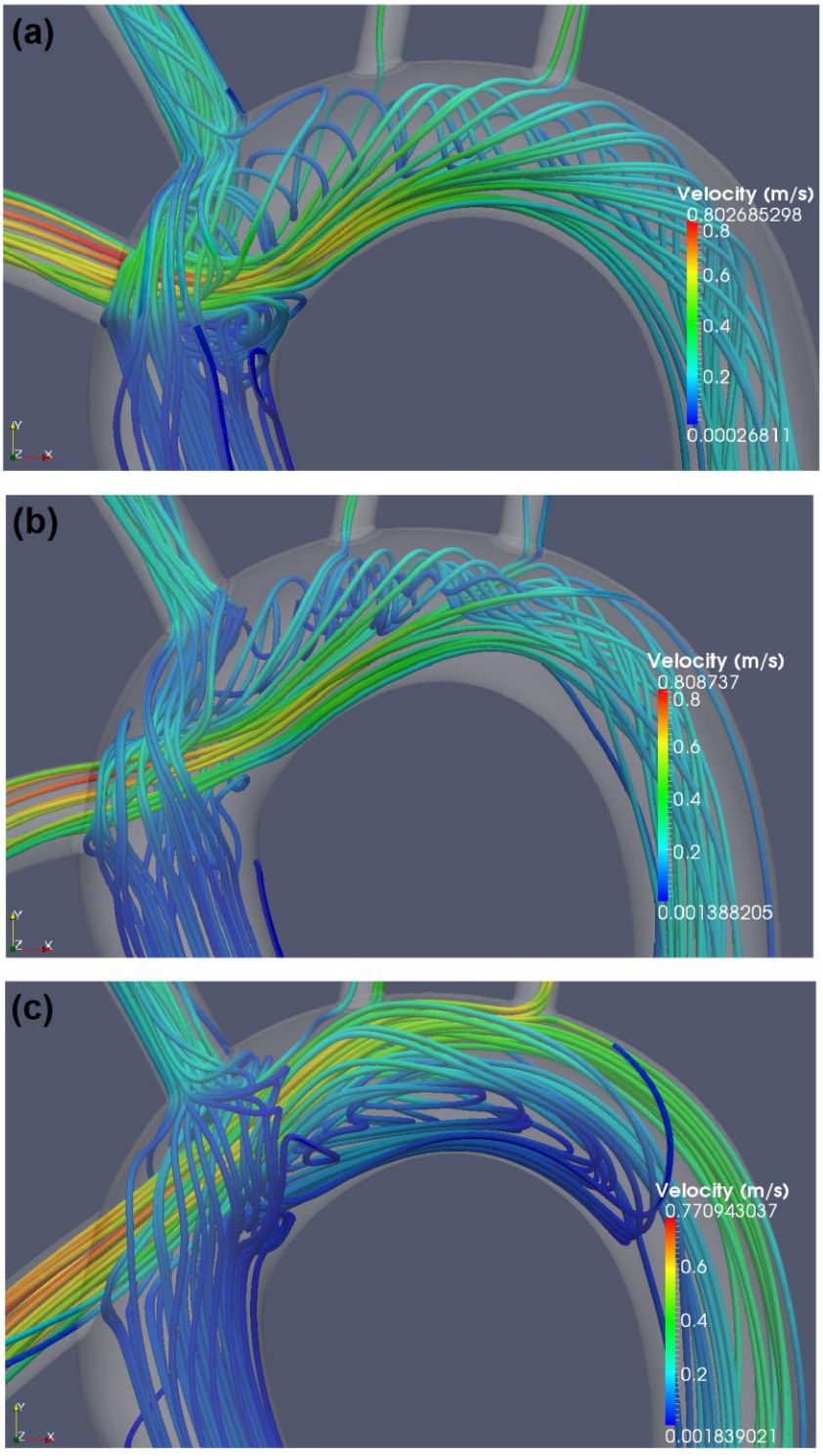

Figure 10: Streamlines colored by velocity for the vectors for the (a) β = 90°, (b) 60° and (c) 30° no bypass cases

The recirculation zones are better visualized by using velocity streamlines, shown in Figure 10 for the three no bypass cases. Figure 10a clearly shows the large, slower moving recirculation zone created by the cannula impingement jet on the aortic wall for the $\beta = 90^{o}$ orientation. The recirculation zone for the $\beta = 60^{o}$ orientation (Figure 10b) is less pronounced than the $\beta = 90^{o}$ case as shown by the streamlines but is still present. By changing the cannula implantation angle to $\beta = 30^{o}$ (Figure 10c), the recirculation zone is shifted further downstream and occupies a much larger region of the aortic arch. This much larger recirculation introduces significant flow reversal and, if caught in this recirculation, blood clots are thrown back upstream. On occasion, clots that were traveling down the descending aorta had their path reversed by this recirculation zone and ended up in right subclavian artery and ultimately traveling to the right vertebral artery resulting in stroke.

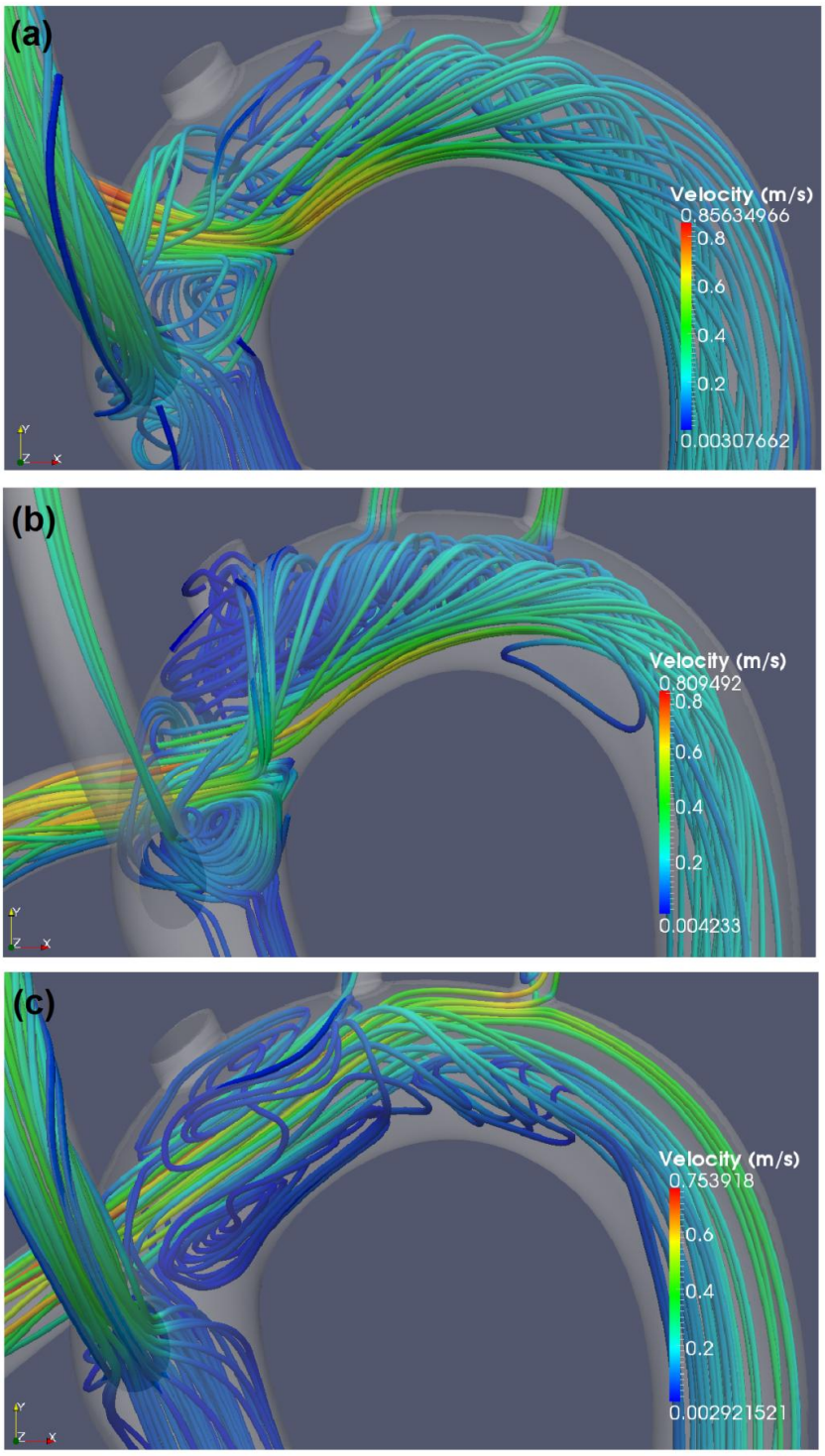

Figure 11: Streamlines colored by velocity for the vectors for the (a) β = 90°, (b) 60° and (c) 30° IA bypass cases

Velocity streamlines for the IA bypass configurations are provided in Figure 11. It can be seen that the flow fields for the 90^o and 60^o IA bypass orientations are very similar to their no bypass counterparts. Figure 11b shows a larger recirculation zone than seen in the no bypass case of the same 60^o orientation (Figure 10b). This may be due to the fact that a smaller fraction of the ascending aorta blood flow is seen at the same location as the no bypass case because the IA bypass removes some of that flow. Thus, it's easier for a recirculation zone to form. Interestingly, it seems the IA bypass has augmented the recirculation zone for all of the cannula orientations. Once the flow is recirculated, it has nowhere to go due to the blockage applied at the IA takeoff. This augmentation is most notably seen in Figure 11b and 11c. Significant swirling is seen in before the IA takeoff and offers another zone for particle "re-randomization".

One of the most important inferences to be taken from Figure 11a and 11b is that, for this bypass implantation location, the IA bypass is actually hurting rather than helping. The recirculation zones caused by the 60^o and 90^o cannula orientations impinging on the aortic wall are sitting right below the IA bypass implantation site. After thrombi flow through the cannula and impact the aortic wall, there is a strong chance they are recirculated and entrained by the aortic flow moving through the IA bypass and ultimately ending up in either the right subclavian, vertebral or carotid artery. The 30^o cannula orientation offers no such chance; the recirculation zone in this case is far removed from the IA implantation site. The LCA bypass cases (Figure 12) have similar flow fields when compared with the IA bypass cases and suffer from similar drawbacks. However, due to the lower position and smaller diameter of the LCA bypass conduit, there is an overall smaller chance of embolization in all cannula orientations (see Table 1).

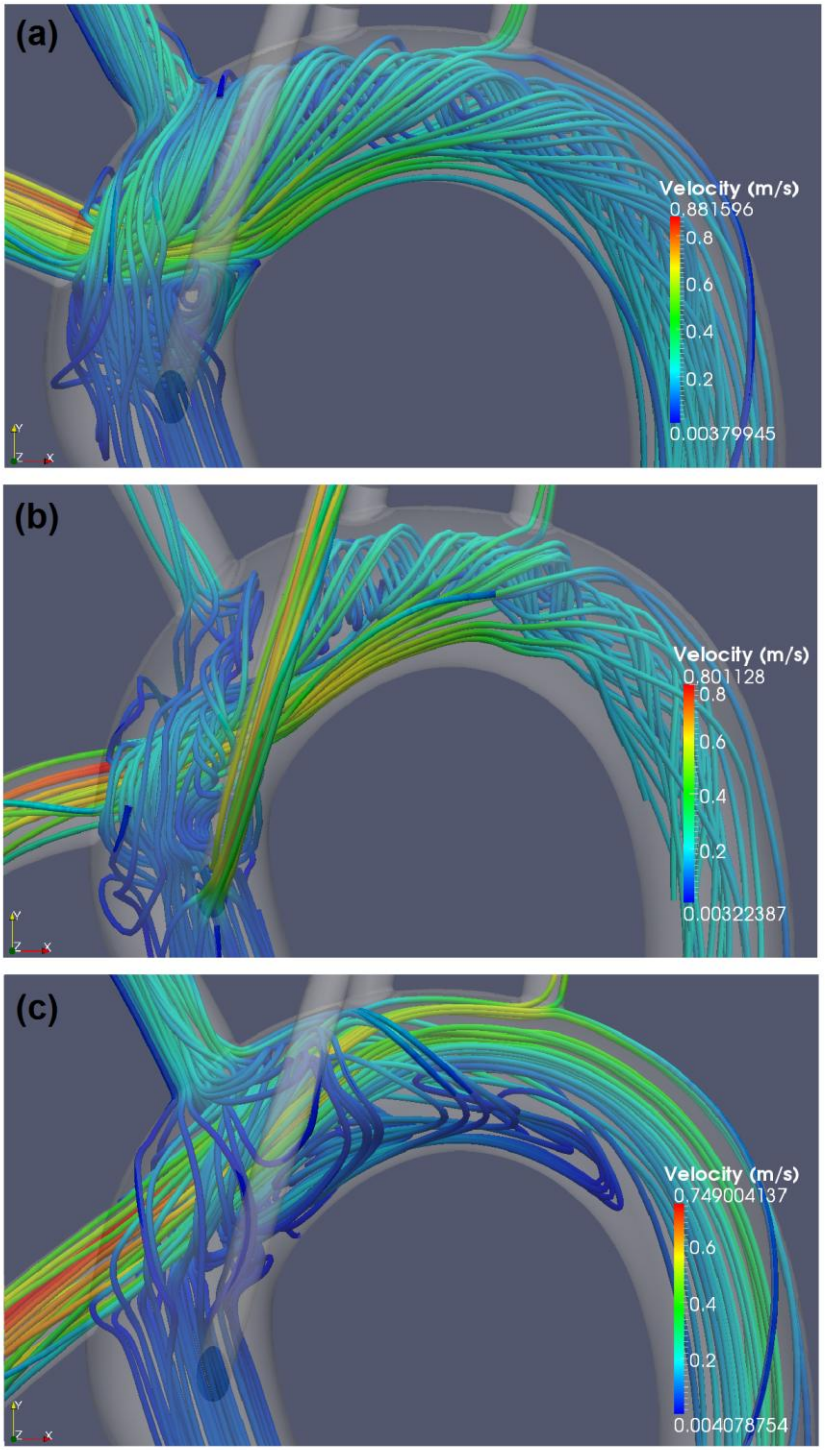

Figure 12: Streamlines colored by velocity for the vectors for the (a) β = 90°, (b) 60° and (c) 30° LCA bypass cases

When discrete particles are present in fluid flow, the particles have the possibility of either follow fluid streamlines or, due to momentum, follow their own unique trajectory. This behavior can be quantified by calculating the Stokes (St) number for the particle. Intuitively, smaller particles will tend to follow fluid streamlines while larger particles follow their own trajectory. The Stokes number is defined as

$$St = \frac{\rho_p {d_p}^2 U}{18 \mu_f D}$$

where ρ_p is the density of the particle, d_p is the particle diameter, U is the fluid velocity, μ_f is the fluid viscosity and D is the diameter of the enclosing vessel. Particles with a Stokes number less than unity have the tendency to follow fluid streamlines while a Stokes number larger than unity denotes the particle's tendency to depart from fluid streamlines. Stokes number contour plots for all LVAD orientations and bypass cases have been calculated using the post processing software Paraview 3.14.1. The plots are calculated using one vessel diameter value, an average aortic arch diameter, and thus are only valid in the aortic arch. Because the flow velocity values are relatively constant across the standard, LCA and IA bypass cases of the same LVAD orientation, the Stokes number plots for all particle sizes are similar and only the base cases ($\beta = 90^o$, 60^o and 30^o) are provided.

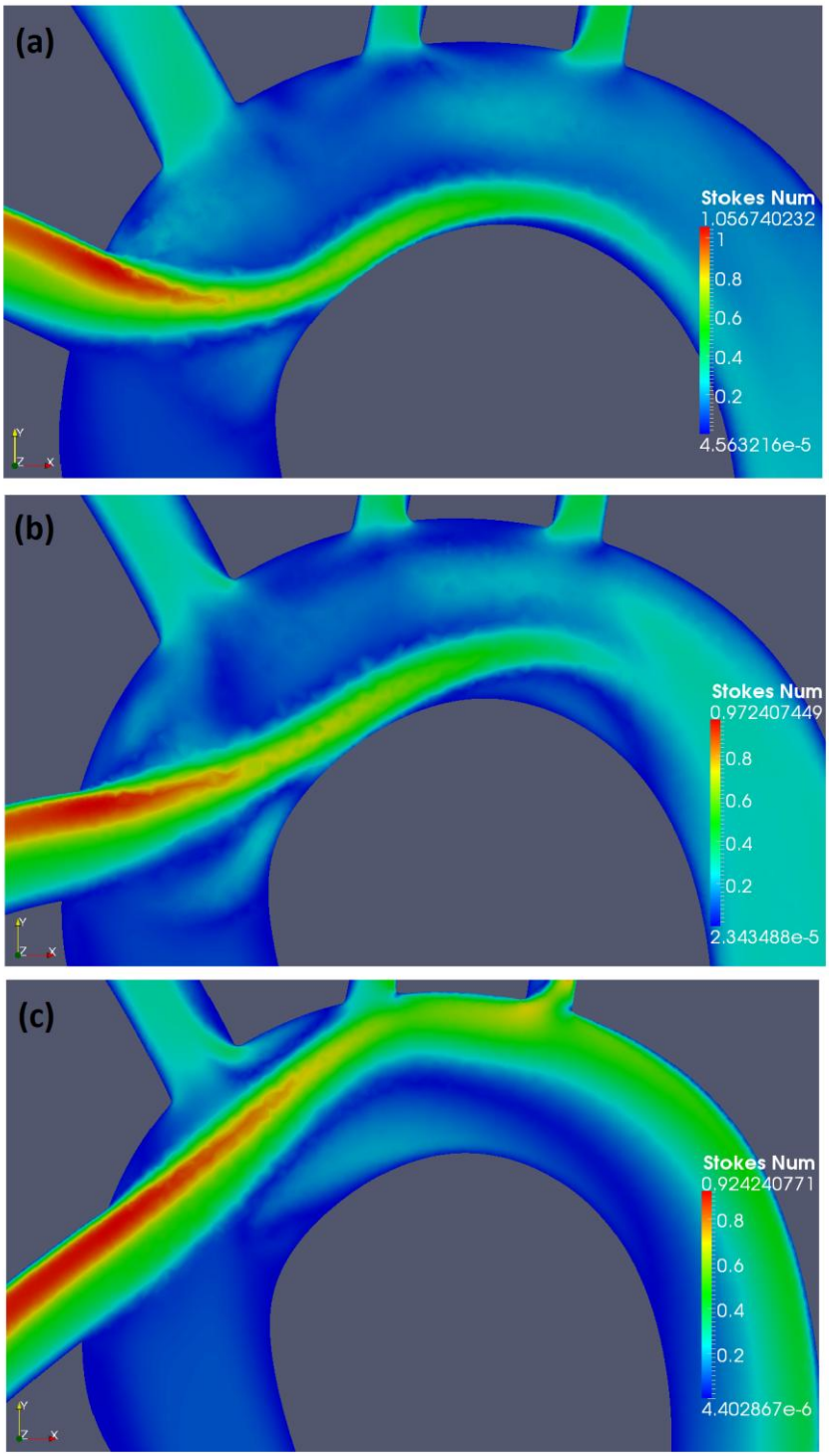

Figure 13: Stokes number plots for (a) β = 90°, (b) 60° and (c) 30° no bypass cases, 1mm particle diameter

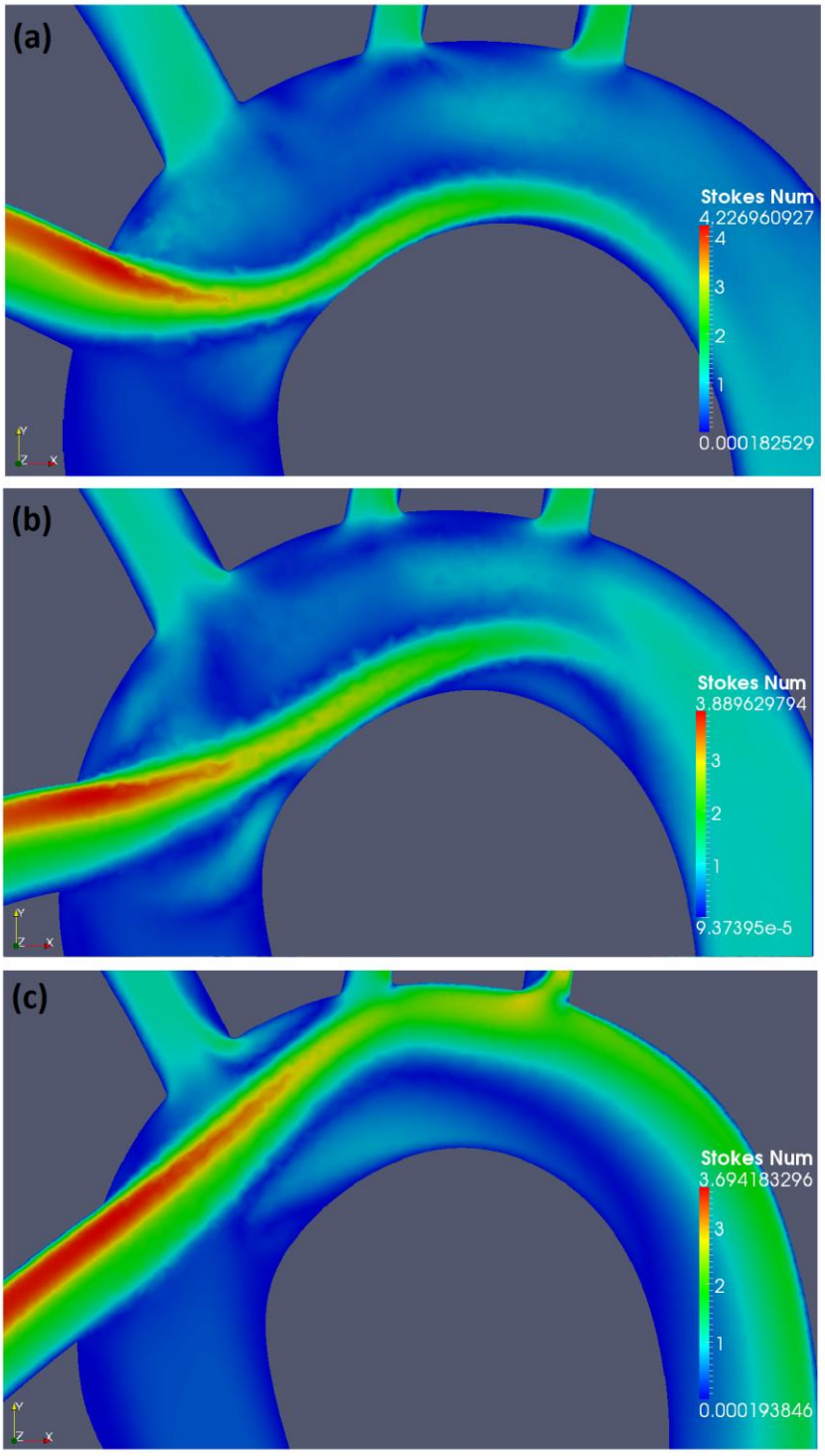

Figure 14: Stokes number plots for (a) β = 90°, (b) 60° and (c) 30° no bypass cases, 2mm particle diameter

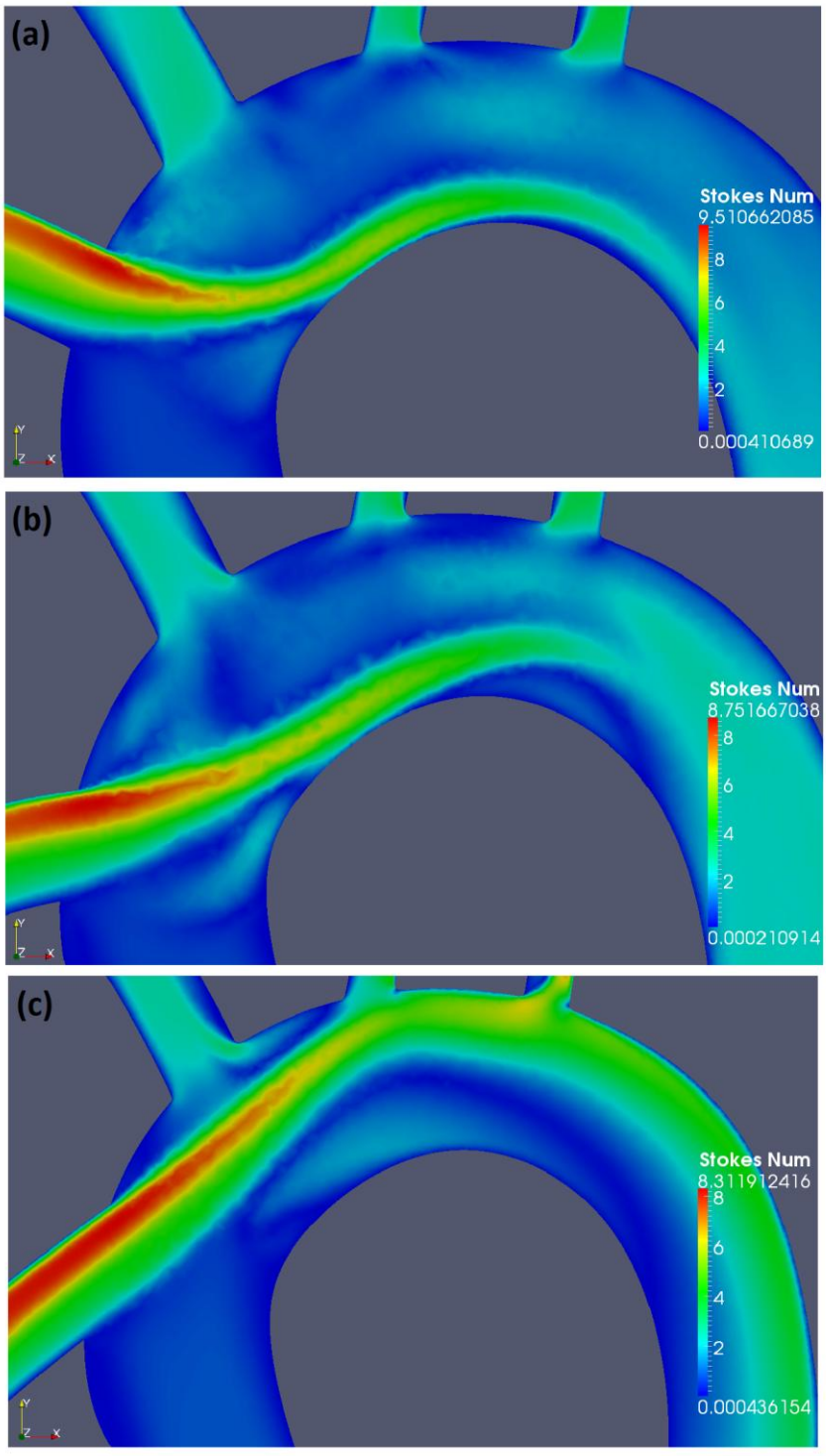

Figure 15: Stokes number plots for (a) β = 90°, (b) 60° and (c) 30° no bypass cases, 3mm particle diameter

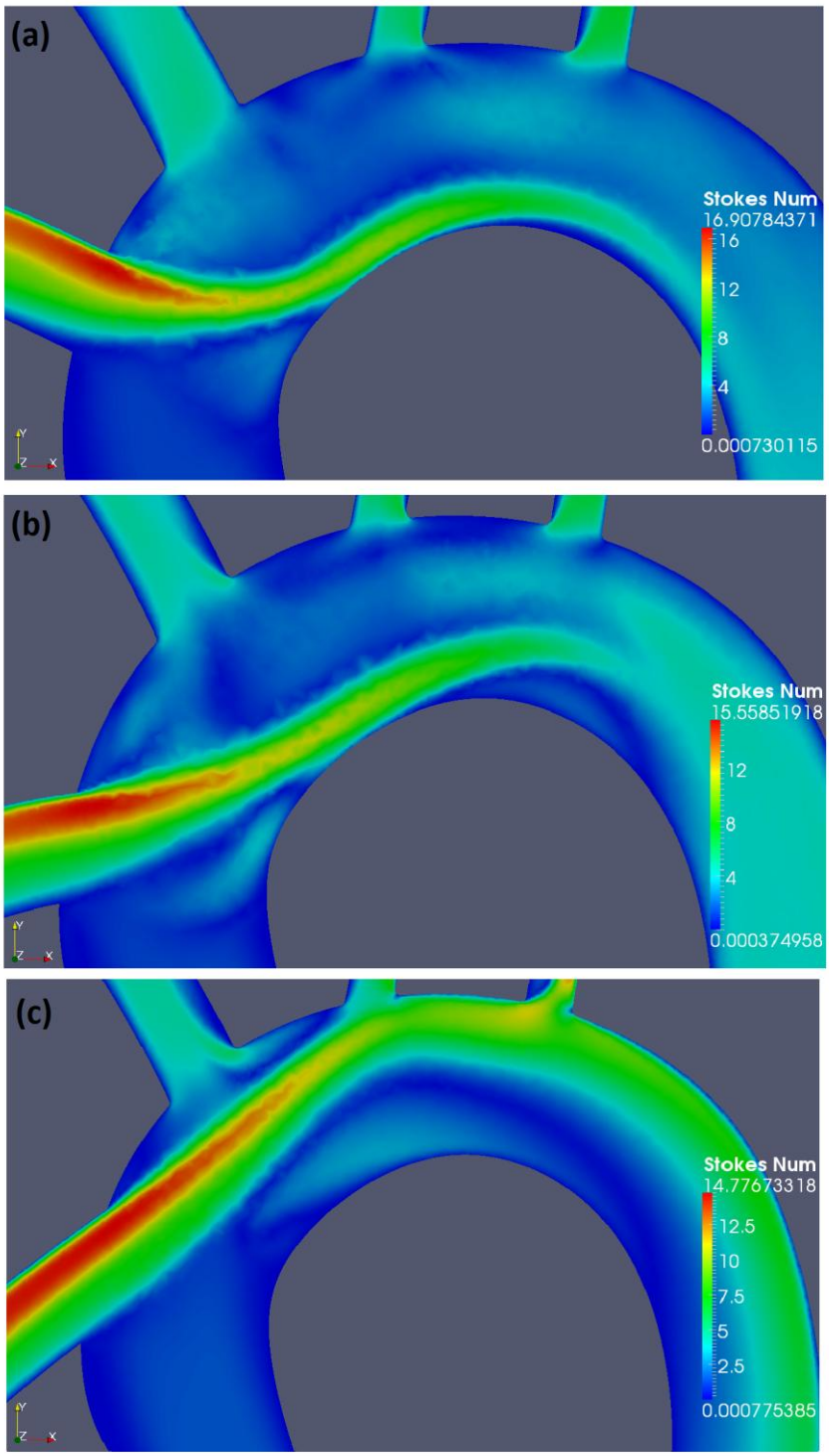

Figure 16: Stokes number plots for (a) β = 90°, (b) 60° and (c) 30° no bypass cases, 4mm particle diameter

The Stokes number contour plots for a particle diameter of 1mm are shown in Figure 13. It can be seen that a maximum Stokes number of approximately 1, in all LVAD orientations, is achieved right as the particles enter the aortic arch. As the thrombi travel into the aortic arch, their Stokes number drops below 1. This means that the 1mm particles will have the tendency to follow the fluid streamlines; if the particle is entrained by a streamline headed to the inominate artery, that's where it will end up. The Stokes number contour plots for a 2mm particle diameter are shown in Figure 14. Upon entering the aortic arch, the particles experience Stokes numbers ranging from 3 to 4 and the number drops quickly to around 2. Therefore, the 2mm particles will have the tendency to be governed by momentum but the distinction between the two regimes is weak. Once in the core of the aortic flow, however, the Stokes number drops below 1. If any particles are recirculated, as is the case with the $\beta = 90^{o}$ and $\beta = 60^{o}$ orientations, the particles' trajectory will be determined by fluid streamlines. The Stokes number plots for 3mm and 4mm particle diameters are shown in Figures 15 and 16, respectively. For these particle sizes, it is likely that their trajectory will be governed by momentum and is less affected by the aortic arch streamlines. Even in the core aortic flow, Stokes numbers for these particle sizes stay above unity.

In the context of Stokes numbers, the trend followed by the results in Table 1 becomes apparent. 1 and 2mm thrombi diameters are more likely to follow streamlines than the 3 and 4mm thrombi diameters. As a result, those particle sizes result in more stroke occurrences. The 1 and 2mm particle diameter stroke percentages are within 5% for each LVAD orientation. It should also be noted that the 2mm particles consistently caused a lower stroke risk due to the overall higher Stokes number, and thus a larger fraction of the 2mm particles flowing down the

descending aorta. The larger Stokes numbers for the 3 and 4mm thrombi mean that the particles will likely be governed by momentum rather than flow streamlines. According to Figures 15 and 16, the Stokes numbers of the core aortic flow are around 1 or 2. This means that recirculated 3 or 4mm diameter particles have the tendency to follow the momentum imparted by the core flow and are less likely to break off and flow into the aorta's branching arteries. The 3 and 4mm particles that remain in the LVAD cannula jet experience Stokes numbers well above 1 and thus follow their trajectory down the descending aortic arch. Table 1 shows a large decrease in stroke occurrence between the 2 and 3mm particle diameters for all cases. This is due to the larger particles having larger Stokes numbers and following the trajectory imparted by the cannula jet straight down the descending aorta.

CHAPTER 4: DISCUSSION AND CONCLUSIONS

Based on the previous discussion, it is apparent that the addition of an LVAD cannula alone significantly alters the flow inside of the aortic arch. The implantation angle has also been seen to have a large effect on the flow field as well. In all LVAD orientation cases, flow is recirculated. In the $\beta = 90^o$ and $\beta = 60^o$ orientations, the recirculation is due to the cannula flow impinging on the inner aortic wall on the lower portion of the arch. The recirculation seen in the $\beta = 30^o$ orientation is due to flow separation caused by the downward turn of the aortic arch toward the descending aorta. These recirculation zones act as "randomizer" for the thrombi, causing them to travel to vessel they may not have gone to otherwise. In the $\beta = 30^o$ orientation, thrombi were seen to completely reverse their trajectory and travel upstream to the inominate artery.

What is the most effective LVAD cannula orientation angle?

According to Table 1, the percentages of embolization are very similar for the $\beta = 60^o$ and $\beta = 90^o$ orientation (no bypass) across all of the particle sizes studied. This is likely due to the similar recirculation pattern as the cannula jet contacts the inner aortic wall. Figures 9a, 9b, 10a and 10b show this recirculation zone. The recirculation for the $\beta = 60^o$ orientation is reduced when compared with the $\beta = 90^o$ orientation however it is significant enough to effect thrombus trajectory.

The $\beta = 30^o$ orientation does not cause the same recirculation pattern as seen in the $\beta = 90^o$ and $\beta = 60^o$ orientations. The cannula jet completely bypasses the inner aortic wall and impacts the aorta near the LCA takeoff. This causes flow separation from the inner aortic arch

and a much larger recirculation zone is created. Despite this large recirculation zone, the $\beta = 30^o$ orientation (no bypass) consistently results in significantly lower embolization rates than the $\beta = 90^o$ and $\beta = 60^o$ orientations. The cannula jet overshoot deposits thrombi at the ideal location to travel through the descending aorta to the less harmful lower body location and away from the high stroke risk carotid and vertebral arteries. As seen in Figure 9c, the cannula jet has the possibility of depositing thrombi at the takeoff for the LCA. If β was slightly larger than 30^o, possibly 35^o or 40^o, then the cannula jet would just touch the inner aortic wall and intersect the outer aortic wall at the LSA takeoff, delivering thrombi to the less lethal left subclavian artery and descending aorta.

Should AO-IA or AO-LCA bypasses be implemented?

The use of an AO-IA or AO-LCA bypass has the ability to either increase or decrease the embolization rates as far as single particle sizes are concerned. In the $\beta = 30^o$ orientation, an AO-LCA bypass noticeably improved embolization rates over the no bypass case for 1mm. However, it also increased the rate of 4mm particle embolization. In the $\beta = 90^o$ orientation, the AO-LCA bypass significantly reduced 1mm and 2mm stroke occurrence when compared with the AO-IA and no bypass cases.

Generally, bypasses did not alter embolization rates significantly on the overall scale. The $\beta = 60^o$ and $\beta = 30^o$ orientations showed very minor changes to particle destinations when a bypass was used. The $\beta = 90^o$ orientation was most effected by a bypass scenario; the AO-LCA bypass decreased the embolization rate by roughly 2% while the AO-IA bypass increased the embolization rate by approximately 2%. The LVAD orientation of the most interest is the $\beta =$

30^o orientation as it resulted in the lowest overall embolization rates. In this case, the bypasses offer no real advantage so their implementation is not recommended.

Closing thoughts and future work

The pediatric aortic arch geometry used in the study was entirely synthetic and created based on characteristic aortic arch dimensions of a 20 kg baby. In reality, variances in these dimensions occur. As a result, the best solution for the synthetic geometry may not be the best solution for each person. The determination for the optimum LVAD cannula implantation angle will be best determined on a patient specific basis.

This study does not address the possibility for thrombi to be formed inside of the aorta due to the stagnation regions caused by the LVAD cannula. Thrombi are known to form inside of the left ventricle because of the flow pattern changes caused by the presence of the LVAD so there is a chance the same could occur inside of the aorta. This would be most apparent in the $\beta = 30^o$ orientation because of the larger recirculation zone and its stagnation region.

This study also does not include the compliance of the walls that occurs when blood interacts with its surrounding vessels. This fluid structure interaction (FSI) is very computationally expensive and is not a trivial task. Work is currently being done to link the structural program ABAQUS with the CFD program STAR-CCM+ to handle FSI simulations. In the future, LVAD aortic arch simulations will have the ability to include vessel compliance for a more physically accurate realization of the LVAD-thrombus problem.

The effect of gravity on particle destinations is being considered. There are two possible gravity vector orientations: standing up and laying down. Preliminary particle track results show

some differences between a case including gravity and a case neglecting it. For a "lying down" gravitational orientation with the $\beta = 90^{o}$ cannula angle, the 1mm particle statistics were similar to those made without gravity being considered. The 2mm to 4mm particle statistics started to stray from the no-gravity case. At this point, the full effect of the force of gravity on thrombi destinations is not known but the topic will be investigated further and the importance of gravity will be determined.

REFERENCES

Andres F. Osorio, Ruben Osorio, Andres Ceballos, Reginald Tran, William Clark, Eduardo A. Divo, I. Ricardo Argueta-Morales, Alain J. Kassab & William M. DeCampli (2011): Computational fluid dynamics analysis of surgical adjustment of left ventricular assist device implantation to minimize stroke risk, Computer Methods in Biomechanics and Biomedical Engineering, DOI:10.1080/10255842.2011.629616

"ANSYS FLUENT 6.3 Documentation." *FLUENT 6.3 Documentation*. N.p., n.d. Web. 18 May 2012. <http://hpce.iitm.ac.in/website/Manuals/Fluent_6.3/fluent6.3/help/index.htm>.

Bakker, Andre. "Applied Computational Fluid Dynamics." Lecture.

Duncan, Brian W. "Pediatric Mechanical Circulatory Support in the United States: Past, Present, and Future." *American Society of Artificial Internal Organs* (2009): n. pag. Web.

Fraser, Charles D., Kathleed E. Carberry, Richard Owens, Karol A. Arrington, David L.S Morales, Jeffery S. Heinle, and Dean McKenzie. "Preliminary Experience With the MicroMed DeBakey Pediatric Ventricular Assist Device." *Pediatric Cardiac Surgery Annual* (n.d.): n. pag. Web.

Imamura, Michiaki, Amy M. Dossey, Parthak Prodhan, Michael Schmitz, Elizabeth Frazier, Umesh Dyamenahalli, Adnan Bhutta, Robert Morrow, and Robert Jaquiss. "Bridge to Cardiac Transplant in Children: Berlin Heart versus Extracorporeal Membrane Oxygenation." *Annals of Thoracic Surgery* (2009): n. pag. Print.

Kormos, Robert L., and Leslie W. Miller. *Mechanical Circulatory Support: A Companion to Braunwald's Heart Disease*. N.p.: n.p., n.d. Print.

Layton, K.F., D.F. Kallmes, H.J. Cloft, E.P. Lindell, and V.S. Cox. "Bovine Aortic Arch Variant in Humans: Clarification of a Common Misnomer." *American Journal of Neuroradiology* (2006): n. pag. Web. <http://www.ajnr.org/content/27/7/1541.full>.